



OPEN ACCESS

EDITED BY

Long Li,
University of Alberta, Canada

REVIEWED BY

Cyril Aubaud,
UMR7154 Institut de Physique du Globe
de Paris (IPGP), France
Kan Li,
Woods Hole Oceanographic Institution,
United States

*CORRESPONDENCE

Maoliang Zhang,
mzhang@tju.edu.cn
Sheng Xu,
sheng.xu@tju.edu.cn

SPECIALTY SECTION

This article was submitted to
Geochemistry,
a section of the journal
Frontiers in Earth Science

RECEIVED 06 November 2022

ACCEPTED 25 November 2022

PUBLISHED 19 January 2023

CITATION

Liu Y, Liu W, Zhou X, Zhong J, Zhang M
and Xu S (2023), Carbon mobilization
in response to the 2021 M_w 7.4 Maduo
earthquake: Constraints from carbon
isotope systematics of subsurface fluids.
Front. Earth Sci. 10:1091052.
doi: 10.3389/feart.2022.1091052

COPYRIGHT

© 2023 Liu, Liu, Zhou, Zhong, Zhang and
Xu. This is an open-access article
distributed under the terms of the
[Creative Commons Attribution License
\(CC BY\)](https://creativecommons.org/licenses/by/4.0/). The use, distribution or
reproduction in other forums is
permitted, provided the original
author(s) and the copyright owner(s) are
credited and that the original
publication in this journal is cited, in
accordance with accepted academic
practice. No use, distribution or
reproduction is permitted which does
not comply with these terms.

Carbon mobilization in response to the 2021 M_w 7.4 Maduo earthquake: Constraints from carbon isotope systematics of subsurface fluids

Yi Liu¹, Wei Liu¹, Xiaocheng Zhou², Jun Zhong¹,
Maoliang Zhang^{1,3*} and Sheng Xu^{1*}

¹School of Earth System Science, Tianjin University, Tianjin, China, ²Institute of Earthquake Forecasting, China Earthquake Administration, Beijing, China, ³Atmosphere and Ocean Research Institute, The University of Tokyo, Chiba, Japan

Active fault zones provide favorable channels for the discharge of carbon-bearing fluids from Earth's interior. Earthquakes, as a common fault-related dynamic process, can disturb the circulation of subsurface fluids and their interactions with country rocks and sediments on short timescales, which may cause changes in carbon mobilization processes and carbon sources of the discharged fluids. However, quantitative research on earthquake-induced changes in carbon mobilization at deep and shallow levels remains lacking. Here, we present a quantitative study on stable carbon isotopes ($\delta^{13}\text{C}$) and radiocarbon values ($\Delta^{14}\text{C}$) of dissolved inorganic carbon (DIC) in subsurface fluid samples from the surface rupture zone formed by the M_w 7.4 Maduo earthquake (22 May 2021) and the East Kunlun fault, NE Tibetan Plateau. Our results show that $\delta^{13}\text{C}_{\text{DIC}}$ values vary from -11.6% to 0.1% , while $\Delta^{13}\text{C}_{\text{DIC}}$ values have a range of -980% to -46% . Using a mass balance model based on $\delta^{13}\text{C}_{\text{DIC}}$ and DIC concentrations, we calculated the proportions of source components involved in DIC, including organic carbon, carbonates, and deeply-sourced carbon. On average, waters discharging from the surface rupture zone have higher inputs from organic carbon (28.1%) than those from the East Kunlun fault (18.6%), with the latter showing higher deeply-sourced carbon contributions (45.7% vs. 30.7%). This is consistent with the lower average $\Delta^{14}\text{C}_{\text{DIC}}$ value (-544%) observed from the East Kunlun fault, suggesting more inputs from carbon source components that are devoid of ^{14}C (i.e., deeply-sourced carbon and carbonates). These findings indicate that seismic events can significantly affect the carbon mobilization processes at variable depths, especially the shallow soil organic carbon in the case of the 2021 Maduo earthquake. The potential effects of earthquake-induced changes in carbon mobilization processes should be taken into account in the modeling of tectonic carbon dioxide degassing and carbon cycle on longer timescales.

KEYWORDS

carbon mobilization processes, carbon isotope systematics, dissolved inorganic carbon, subsurface fluids, Maduo earthquake

1 Introduction

The discharge of carbon-bearing fluids is prevalent in active fault zones controlled by different tectonic regimes (e.g., Becker et al., 2008; Tamburello et al., 2018; Zhang et al., 2021). Previous studies indicate that active fault zone can act as a favorable channel for fluid transfer from Earth's interior to the surface (Williams et al., 2013), or as a barrier for fluid flows in the case of episodic fluid accumulation within fault-related traps (Miller et al., 2004; Han et al., 2019). The circulation of subsurface fluids in the active fault zones, as well as their interaction with country rocks or sediments at variable depths, is thus expected to affect the geochemical compositions of groundwaters (Newell et al., 2008; Crossey et al., 2009). Such fluid-rock or fluid-sediment interactions have established the basis for earthquake forecasting studies that integrate the geochemistry of subsurface fluids (e.g., natural spring waters) as an effective tool for evaluating the potential earthquake risk (Ingebritsen and Manga, 2014).

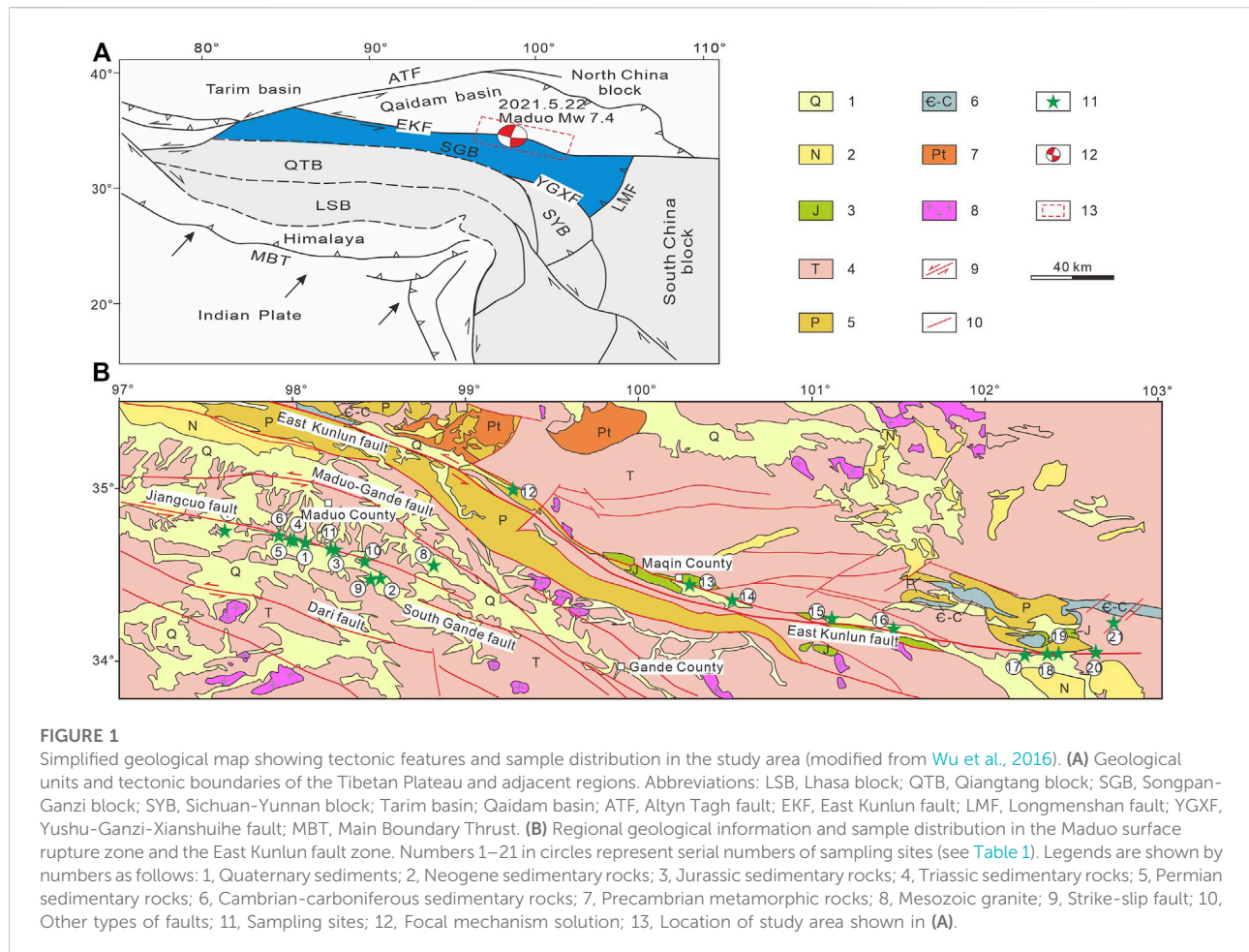
The kinematics and locking status of seismically active fault zones play an important role in controlling the decarbonation reactions of source materials and the migration of carbon-bearing fluids through the lithosphere (Faulkner et al., 2010; Zucchi, 2020). At a regional scale, the correlations between deeply-sourced CO₂ emissions, seismic activity, and fault types have been clearly demonstrated (Tamburello et al., 2018). Moreover, numerous studies have reported post-earthquake perturbations in geochemistry and fluxes of carbon-bearing fluids associated with specific earthquake events (e.g., Claesson et al., 2004; Skelton et al., 2014; Ünal-İmer et al., 2016; Girault et al., 2018; Bonini, 2022). From a dynamic point of view, earthquakes have the potential to disturb the circulation of subsurface fluids and their leaching effects on country rocks or sediments over short timescales (Rosen et al., 2018), giving rise to transient changes in geochemical proxies of the discharging fluids along active faults, such as concentrations and isotopic compositions of dissolved inorganic carbon (DIC) (Girault et al., 2018; Barbieri et al., 2020). As a result, carbon isotope systematics (e.g., $\delta^{13}\text{C}_{\text{DIC}}$ and $\delta^{13}\text{C}_{\text{CO}_2}$; Barbieri et al., 2020) of deeply-sourced fluids, together with other hydrogeochemical and isotopic tracers (e.g., Cl⁻, SO₄²⁻, and ³He/⁴He; Tsunogai and Wakita, 1995; Kulongoski et al., 2013; Bräuer et al., 2014), have been taken as potential precursors to earthquakes. Nevertheless, quantification of the earthquake-induced changes in carbon mobilization processes at deep and shallow levels remains loosely constrained, especially for earthquakes that occurred in the continental orogenic setting of the Tibetan Plateau and its surrounding regions.

In this study, we focus on carbon source quantification of a post-earthquake sample set of subsurface fluids from Maduo region in the Songpan-Ganzi block of NE Tibetan Plateau

(Figure 1), based on stable carbon isotopes ($\delta^{13}\text{C}$) and radiocarbon values ($\Delta^{14}\text{C}$) of total DIC, which can contribute to understanding the carbon mobilization processes in response to the M_w 7.4 Maduo earthquake (98.34°E, 34.59°N, epicenter depth = 17 km; Zhu et al., 2021) occurred on 22 May 2021. The data of water chemistry, $\delta^{18}\text{O}_{\text{H}_2\text{O}}$, $\delta\text{D}_{\text{H}_2\text{O}}$, and ⁸⁷Sr/⁸⁶Sr of this sample set were reported in Lu et al. (2021), but carbon isotope systematics of DIC have not been investigated, resulting in an open question about the DIC sources and carbon mobilization mechanism associated with the 2021 Maduo earthquake. Spatially, carbon sources of subsurface fluids from boundary faults of the Songpan-Ganzi block (e.g., Yushu-Ganzi-Xianshuihe fault and Longmenshan fault; Figure 1A) have been reported (e.g., Zhou et al., 2015; Tian et al., 2021; Liu et al., 2022; Xu et al., 2022). In contrast, the carbon source components of the Jianguo fault in the block interior (Figure 1B), which was ruptured by the 2021 Maduo earthquake, are still largely unknown. Our results show that earthquake-induced changes in mobilization of soil organic carbon are prominent for the fluids discharging from the Maduo surface rupture zone, compared to the adjacent East Kunlun fault zone that is characterized by discharge of carbon-bearing fluids with more contributions from deeply-sourced carbon.

2 Geological background

Since the early Cenozoic, the continuous India-Asia continental collision has resulted in extensive crustal shortening, tectonic uplift, and lateral extrusion of the micro-continental blocks that constitute the Tibetan Plateau (Tapponnier et al., 2001). As a result, a series of active fault zones were formed primarily along the block boundary and also in the block interior (Figure 1). Generally, tectonic deformation of the block boundary faults controls outward expansion of the Tibetan Plateau and the occurrence of high-frequency strong earthquakes within the continental interiors (Liu and Stein, 2016). Our study area is located in the Songpan-Ganzi block, which is bounded by the East Kunlun fault to the north, the Yushu-Ganzi-Xianshuihe fault to the south, the Longmenshan fault to the east, and the western segment of the Altyn Tagh fault to the west (Figure 1A). There are a series of left-lateral strike-slip faults inside of the Songpan-Ganzi block near the East Kunlun fault zone, including the Maduo-Gande fault, Jianguo fault, South Gande fault, and Dari fault from north to south (Figure 1B). Permian and Triassic strata and Quaternary alluvial diluvium are mainly exposed in the study area; the main lithology assemblage includes sandstone, glutenite, limestone, slate, pyroclastic rock and sand gravel (Figure 1B).



As one of the most seismically active regions in mainland China, the boundary faults of the Songpan-Ganzi block, eight large earthquakes (mostly $M > 7.0$) have occurred in the past 25 years (Pan et al., 2022), the largest of which was the 2008 M_w 7.9 Wenchuan earthquake (Hubbard and Shaw, 2009). Located to the NE of the 2021 Maduo earthquake, the East Kunlun fault is a large-scale left-lateral strike-slip fault with an inclination angle of about $55\text{--}85^\circ$ and a total length of about 1900 km (Figure 1A). The slip rate of this fault decreases from 11 mm/yr to 2 mm/yr from east to west (Ren et al., 2013), which is still in an active state of intensive seismicity. A recent study by Yue et al. (2022) suggests that the Songpan-Ganzi block, although being controlled by a distributed shearing stress state, exhibits slip rates on its boundary faults (e.g., ~ 10 mm/y for the Xianshuihe fault) about one order of magnitude higher than that on the block interior faults (0–2 mm/y). The 2021 M_w 7.4 Maduo earthquake occurred along the Jianguo fault in the block interior (Pan et al., 2022), making it a relatively rare case of strong earthquake in the interior of the Songpan-Ganzi block.

Importantly, the 2021 Maduo earthquake provides a good opportunity for constraining the carbon sources of subsurface

fluids and their changes in response to strong earthquakes in the block interior. After the Maduo earthquake on 22 May 2021, a nearly 70-km-long surface rupture zone with a NWW-SEE strike was formed along the Jianguo fault (Figure 1B), which is characterized by linear distribution of passes, fault triangles, gullies dislocation, twisted ridges, sag ponds, and the discharging spring waters near the surface rupture zone (Lu et al., 2021). The strong rupturing creates favorable conditions for the upward migration of subsurface fluids and controls the NWW-SEE trending distribution of springs (Figure 1B). These newly formed springs are considered in this study to make a comparison of quantitatively constrained carbon sources with natural springs along the East Kunlun fault zone.

3 Samples and methods

In May 2021, twenty-one spring water and surface water samples were collected from the surface rupture zone near the epicenter of the 2021 Maduo earthquake and the East Kunlun fault zone (Figure 1). Among them, nine samples (MDW1–6 and

MDW9–11) are from the Maduo surface rupture zone, and ten samples (MDW12–21) are from the East Kunlun fault zone. For comparison, two surface water samples were collected from the Eling Lake (MDW7) and the Yellow River (MDW8). A portable water parameter meter was used to measure the temperature and pH value of waters. All samples were stored in polyethylene bottles. Based on the data of water chemistry (cations and anions), basicity, temperature, and pH value (Lu et al., 2021), the partial pressure of carbon dioxide ($p\text{CO}_2$) and DIC concentration in water are calculated using software PHREEQC.

The stable carbon isotope and radiocarbon isotope compositions were analyzed in School of Earth System Science, Tianjin University. The stable carbon isotope of DIC was analyzed by the conventional stable isotope ratio mass spectrometer (Model Delta V Plus, Thermo Fisher, United States) coupled with a Gas Bench. 1 mL 85% phosphoric acid was injected into a glass reaction flask, which was purged with high-purity helium gas, and then an appropriate amount of water (0.05–0.33 mL in this study) was injected. After complete reaction (>18 h), CO_2 was introduced into the ion source of the mass spectrometer for analysis of $^{13}\text{C}/^{12}\text{C}$ ratio. Meanwhile, the international standard (NBS-18) was used during the analysis. The results were represented by $\delta^{13}\text{C}_{\text{DIC}}$ relative to the V-PDB standard, and the overall uncertainty in repeated measurements of the working standard NBS-18 is $\pm 0.2\text{‰}$ (2σ). For radioactive carbon isotope of DIC ($\Delta^{14}\text{C}_{\text{DIC}}$) analysis, the water samples were injected into pre-evacuated bottles with 85% phosphoric acid. The produced gas was introduced in the vacuum system for separation between CO_2 and H_2O . The purified CO_2 was sealed in vacuum tube filled with iron powder and zinc powder in which the CO_2 gas reacted with zinc under the condition of Fe catalyst and 550°C to form graphite. The graphite was pressed into a sample holder and loaded in the ion source of the 0.5 MV accelerator mass spectrometer (AMS, 1.5SDH-1, NEC, United States) to determine the $^{14}\text{C}/^{12}\text{C}$ ratio. Repeated measurements of the working standards indicate $\sim 0.3\%$ precision and accuracy on the $^{14}\text{C}/^{12}\text{C}$ ratio. The mass-dependent carbon isotopic fractionation effect has been corrected using the on-line AMS-measured $^{13}\text{C}/^{12}\text{C}$ ratios.

4 Results

The analytical results of water samples are summarized in Table 1. The $p\text{CO}_2$ values of the 21 water samples range from 0.0011 to 0.0417 atm, much higher than the local atmospheric $p\text{CO}_2$ value of 0.0003 atm. The $\delta^{13}\text{C}_{\text{DIC}}$ values of spring waters in Maduo surface rupture zone vary from -8.5‰ to -4.6‰ , whereas samples in East Kunlun fault zone have a $\delta^{13}\text{C}_{\text{DIC}}$ range of -11.6‰ to 0.1‰ (Table 1). As a comparison, the $\delta^{13}\text{C}_{\text{DIC}}$

values of the Eling Lake water and Yellow River water are -7.3‰ and -11.3‰ , respectively. The $\Delta^{14}\text{C}_{\text{DIC}}$ values of spring water samples range from -980‰ to -46‰ , and one surface water sample from the Yellow River (MDW8) has a $\Delta^{14}\text{C}_{\text{DIC}}$ value of -58‰ (Table 1).

5 Discussion

5.1 Identification of candidate carbon source components

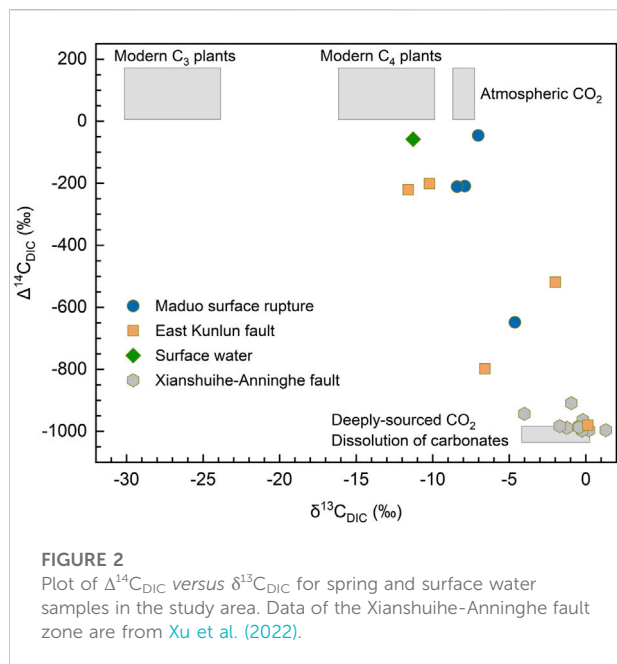
There are generally four candidate carbon end-member for the sources of DIC in spring waters (Chiodini et al., 2000): 1) atmospheric CO_2 ; 2) organic carbon; 3) dissolution of carbonate minerals; 4) deeply-sourced carbon (e.g., mantle-derived and/or metamorphic CO_2). Different carbon source components have specific ranges of $\delta^{13}\text{C}$ values, which on average are -8.5‰ for modern atmospheric CO_2 (Campeau et al., 2017); -26‰ and -12‰ for C_3 and C_4 plants, respectively; -4‰ for mantle-derived CO_2 ; and $0 \pm 2\text{‰}$ for marine carbonate rocks (Telmer and Veizer, 1999; Pineau et al., 2004; Newell et al., 2008). In addition to stable carbon isotope, radiocarbon isotope ($\Delta^{14}\text{C}$) is also an important geochemical indicator for identifying carbon sources (Wang et al., 2022). High $\Delta^{14}\text{C}$ values indicate the involvement of shallow carbon sources such as atmospheric CO_2 and modern organic carbon, while low $\Delta^{14}\text{C}$ values indicate the contribution from deep carbon sources such as carbonate dissolution, mantle-derived CO_2 , and metamorphic CO_2 (Mayorga et al., 2005). Since the stable carbon isotopic compositions of different end-members overlap to some extent, and mixing of any two carbon end-members could lead to $\delta^{13}\text{C}$ values consistent with those of a particular end-member, further identification of carbon source based on stable carbon isotopes and radiocarbon can better constrain the relative contributions of deep and shallow sources of CO_2 (Xu et al., 2022).

According to the relationship between $\delta^{13}\text{C}_{\text{DIC}}$ and $\Delta^{14}\text{C}_{\text{DIC}}$ (Figure 2), compared with the springs in Xianshuihe-Anninghe fault zone (Xu et al., 2022), the springs and surface water in Maduo surface fracture zone and East Kunlun fault zone are basically in the mixing zone of modern organic carbon, atmospheric CO_2 , dissolved carbonate, and deeply-sourced carbon. Most springs near the surface rupture zone are relatively rich in ^{14}C (average $\Delta^{14}\text{C}_{\text{DIC}} = -279\text{‰}$), while most springs near the East Kunlun fault zone are relatively poor in ^{14}C (average $\Delta^{14}\text{C}_{\text{DIC}} = -544\text{‰}$). The $\Delta^{14}\text{C}_{\text{DIC}}$ value of sample MDW21 (-980‰) is basically consistent with those of the springs of Xianshuihe-Anninghe fault zone, falling in the $\Delta^{14}\text{C}_{\text{DIC}}$ range of deeply-sourced carbon and carbonate components (Figure 2). Except for MDW21, the $\Delta^{14}\text{C}_{\text{DIC}}$ values of spring water samples in this study are higher than those of the Xianshuihe-Anninghe samples (-997‰ to -909‰ ; Xu et al., 2022), suggesting more inputs of modern organic

TABLE 1 Sample information, concentrations of major cations and anions, stable carbon isotopes and radiocarbon isotopes of the water samples.

No	Sample ID	Longitude (E)	Latitude (N)	Temperature* (°C)	pH*	Ca ²⁺ (mM)	Mg ²⁺ (mM)	HCO ₃ ⁻ (mM)	SO ₄ ²⁻ (mM)	DIC (mM)	pCO ₂ (atm)	δ ¹³ C _{DIC} (‰)	Δ ¹⁴ C _{DIC} (‰)
1	MDW1	98.086	34.675	8	8.1	1.47	0.77	4.24	0.18	5.13	0.0019	-7.2	
2	MDW2	98.522	34.470	5	7.7	0.67	0.43	2.51	0.04	3.21	0.0029	-7.0	-46
3	MDW3	98.262	34.634	5	8.1	3.13	1.67	8.41	0.81	10.00	0.0035	-8.5	
4	MDW4	98.018	34.694	8	8.3	1.48	1.03	3.97	0.34	4.70	0.0011	-7.9	-209
5	MDW5	98.006	34.695	8	8.2	1.57	0.84	5.02	0.27	6.00	0.0018	-8.2	
6	MDW6	97.932	34.718	5	8.3	2.36	1.17	6.22	0.71	7.33	0.0017	-6.4	
7	MDW7**	97.625	34.750	8	8.2	1.88	0.57	5.03	0.17	6.01	0.0018	-7.3	
8	MDW8***	98.830	34.542	11	8.1	1.56	2.05	6.52	0.08	7.75	0.0030	-11.3	-58
9	MDW9	98.466	34.466	11	8.2	1.36	1.30	3.70	0.36	4.40	0.0013	-4.6	-648
10	MDW10	98.432	34.572	3	8.1	0.93	0.91	3.63	0.10	4.44	0.0016	-5.9	
11	MDW11	98.233	34.643	5	8.2	1.57	0.83	3.96	0.18	4.75	0.0014	-8.4	-211
12	MDW12	99.289	34.985	4.5	8.1	3.64	1.84	6.51	2.16	7.73	0.0027	-2.0	-519
13	MDW13	100.310	34.441	10	8.1	2.52	1.57	7.21	0.78	8.56	0.0032	-6.3	
14	MDW14	100.556	34.357	4.5	8.2	1.64	0.57	4.92	0.07	5.92	0.0017	-11.6	-221
15	MDW15	101.132	34.242	6.5	7.9	2.52	0.84	8.33	0.15	10.19	0.0058	-10.2	-201
16	MDW16	101.488	34.182	9.5	7.8	3.11	0.41	8.15	0.05	10.02	0.0074	-10.9	
17	MDW17	102.266	34.015	9	8.0	2.39	0.83	6.66	0.05	8.03	0.0038	-5.4	
18	MDW18	102.389	34.024	4.5	7.9	2.52	1.12	9.41	0.01	11.53	0.0063	-6.6	-798
19	MDW19	102.458	34.019	12	8.0	1.91	0.89	6.51	0.10	7.85	0.0038	-6.4	
20	MDW20	102.680	34.035	28	8.0	2.17	0.75	7.08	0.10	8.35	0.0051	-3.8	
21	MDW21	102.783	34.203	49	7.6	5.66	2.77	17.8	2.39	20.61	0.0417	0.1	-980

Notes: * Data from Lu et al. (2021); ** Eling Lake water; *** Yellow River water.



carbon to subsurface fluids along the Maduo surface rupture zone and East Kunlun fault zone.

The $p\text{CO}_2$ values in spring and surface waters near the Maduo surface rupture zone and the East Kunlun fault zone are at least over three times higher than the atmospheric CO_2 partial pressure (~ 0.0003 atm; Liu et al., 2022); and therefore, the contribution of atmospheric CO_2 to DIC in the spring and surface waters can be largely excluded. In addition, the infiltrating waters contain a mixed DIC component of atmospheric CO_2 and biospheric organic carbon in the soils, but generally have a $\delta^{13}\text{C}$ value close to the organic carbon end-member (Chiodini et al., 2000). Therefore, the DIC in spring waters is mainly derived from modern organic carbon, carbonate-dissolved carbon, and deeply-sourced carbon. In addition, according to $\Delta^{14}\text{C}_{\text{DIC}}$ values, DIC of MDW2 (-46%) and MDW8 (the Yellow River water, -58%) exhibits clear organic inputs to radiocarbon isotopes, in contrast to the DIC of MDW21 (-980%) that is depleted in ^{14}C due to contributions from deeply-sourced carbon and carbonate dissolution.

5.2 Quantification of carbon source contributions

It is generally accepted that Ca^{2+} and Mg^{2+} dissolved in water (including surface water and groundwater) are mainly derived from dissolution of carbonate minerals (Liu et al., 2022 and references therein), but sulfate minerals may also contribute to part of them (Chiodini et al., 2004). Assuming that Ca^{2+} , Mg^{2+} and SO_4^{2-} in springs are all contributed by dissolution of carbonate and sulfate minerals, the DIC ascribed to carbonate mineral dissolution (C_{carb})

can be calculated according to Eq. 1. After deducting the contribution from carbonate dissolved carbon using Eq. 2, the DIC from external carbon (C_{ext} , non-carbonate dissolved carbon) can be obtained (Chiodini et al., 2000). As shown in Table 2, the C_{carb} and C_{ext} values of spring waters in the Maduo surface rupture zone are $1.05\text{--}3.98$ mmol L^{-1} and $2.09\text{--}6.02$ mmol L^{-1} , respectively, while the C_{carb} and C_{ext} values of spring waters in the East Kunlun fault zone are $2.14\text{--}6.04$ mmol L^{-1} and $3.78\text{--}14.57$ mmol L^{-1} , respectively. According to Eq. 3, the isotopic composition of external carbon can be calculated to further constrain its sources (Chiodini et al., 2004).

$$C_{\text{carb}} = \text{Ca}^{2+} + \text{Mg}^{2+} - \text{SO}_4^{2-} \quad (1)$$

$$C_{\text{ext}} = \text{DIC} - C_{\text{carb}} \quad (2)$$

$$\delta^{13}\text{C}_{\text{DIC}} \times \text{DIC} = \delta^{13}\text{C}_{\text{ext}} \times C_{\text{ext}} + \delta^{13}\text{C}_{\text{carb}} \times C_{\text{carb}} \quad (3)$$

In Eq. 3, $\delta^{13}\text{C}_{\text{ext}}$ represents the isotopic composition of external carbon, and $\delta^{13}\text{C}_{\text{carb}}$ represents the isotopic composition of dissolved carbon from carbonates. The reference $\delta^{13}\text{C}$ value of marine carbonates (0% ; Hoefs, 2009) was used to calculate the isotopic composition of external carbon. In addition, if the water sample before acquisition is affected by CO_2 degassing or carbonate mineral precipitation, the C_{ext} value will be underestimated and the $\delta^{13}\text{C}_{\text{ext}}$ value will be overestimated (Chiodini et al., 2004). The effects of CO_2 degassing or carbonate precipitation on $\delta^{13}\text{C}$ values in springs cannot be constrained based on available data in this study. Nevertheless, following Chiodini et al. (2000), the effect of CO_2 degassing or carbonate precipitation in the calculation is probably negligible when $p\text{CO}_2$ and DIC values are much lower than ~ 1 atm and 0.0695 mol/L, respectively. Considering the DIC concentrations ($3.21\text{--}20.61$ mmol/L) and $p\text{CO}_2$ values ($0.0011\text{--}0.0417$ atm) of water samples in this study (Table 1), we suggest that the effect of significant CO_2 degassing or carbonate precipitation was probably negligible for the calculation of C_{ext} and $\delta^{13}\text{C}_{\text{ext}}$ values in spring waters.

The calculated results (Table 2) show that the $\delta^{13}\text{C}_{\text{ext}}$ values of spring waters in Maduo surface rupture zone range from -15.7% to -9.7% ; the $\delta^{13}\text{C}_{\text{ext}}$ values in the East Kunlun fault zone vary from -18.2% to 0.2% . As shown in Figure 3, the C_{ext} and $\delta^{13}\text{C}_{\text{ext}}$ of springs indicate two candidate sources for external carbon, namely organic carbon and deeply-sourced carbon (i.e., endogenous carbon). The curves represent theoretical mixing of organic carbon end-member with different C_{ext} concentrations and deeply-sourced carbon end-member (Figure 3), which can well explain source components of external carbon in spring waters from the Maduo surface rupture zone and East Kunlun fault zone. In particular, most springs of the East Kunlun fault zone are more enriched in ^{13}C than those from the Maduo surface rupture zone.

The proportions of source components involved in external carbon can be quantitatively constrained by the binary mixing model following Eq. 4.

TABLE 2 Proportions of organic carbon, deeply-sourced carbon, and carbonate involved in DIC of the water samples.

No	Sample ID	Locality	C _{carb} (mM)	C _{ext} (mM)	δ ¹³ C _{ext} (‰)	C _{org} (%)	C _{endo} (%)	C _{carb} (%)
1	MDW1	MSRZ	2.05	3.07	-12.0	28.5	31.4	40.1
2	MDW2	MSRZ	1.05	2.16	-10.4	28.2	39.1	32.7
3	MDW3	MSRZ	3.98	6.02	-14.1	32.9	27.3	39.8
4	MDW4	MSRZ	2.17	2.53	-14.7	30.5	23.3	46.2
5	MDW5	MSRZ	2.14	3.86	-12.7	32.1	32.3	35.6
6	MDW6	MSRZ	2.82	4.51	-10.4	25.6	35.9	38.5
7	MDW7	Eling Lake	2.28	3.74	-11.7	28.8	33.4	37.8
8	MDW8	Yellow River	3.53	4.22	-20.7	42.4	12.1	45.5
9	MDW9	MSRZ	2.31	2.09	-9.8	18.7	28.7	52.6
10	MDW10	MSRZ	1.74	2.69	-9.7	23.8	36.9	39.3
11	MDW11	MSRZ	2.21	2.54	-15.7	32.3	21.2	46.5
12	MDW12	EKFZ	3.31	4.42	-3.5	10.0	47.2	42.8
13	MDW13	EKFZ	3.31	5.25	-10.3	25.4	35.9	38.7
14	MDW14	EKFZ	2.14	3.78	-18.2	44.1	19.8	36.1
15	MDW15	EKFZ	3.22	6.98	-14.9	39.5	29.0	31.5
16	MDW16	EKFZ	3.46	6.56	-16.7	41.8	23.7	34.5
17	MDW17	EKFZ	3.17	4.87	-8.9	22.2	38.4	39.4
18	MDW18	EKFZ	3.63	7.90	-9.6	26.7	41.8	31.5
19	MDW19	EKFZ	2.70	5.16	-9.7	25.9	39.8	34.3
20	MDW20	EKFZ	2.81	5.54	-5.7	16.7	49.7	33.6
21	MDW21	EKFZ	6.04	14.57	0.2	3.3	67.4	29.3

MSRZ, Maduo surface rupture zone; EKFZ, East Kunlun fault zone. For the East Kunlun fault zone, the average proportions of organic carbon (C_{org}), deeply-sourced carbon (C_{endo}), and carbonate (C_{carb}) end-members are 18.6% (3.3–26.7%), 45.7% (35.9–67.4%) and 35.7% (29.3–42.8%), respectively, which do not take into account samples MDW14 to MDW16 due to possible shallow fluid sources that fail to reflect the properties of deep fluid circulation in the East Kunlun fault zone (see details in Section 5.3 of the main text). Similarly, the average proportions of C_{org}, C_{endo}, and C_{carb} calculated for water samples from the Maduo surface rupture zone are 28.1% (18.7–32.9%), 30.7% (21.2–39.1%), and 41.2% (32.7–52.6%), respectively.

$$\delta^{13}\text{C}_{\text{ext}} \times \text{C}_{\text{ext}} = \delta^{13}\text{C}_{\text{org}} \times \text{C}_{\text{org}} + \delta^{13}\text{C}_{\text{endo}} \times \text{C}_{\text{endo}} \quad (4)$$

The results show that the C_{org} and C_{endo} values of springs near the Maduo surface rupture zone are 0.82–3.29 mmol L⁻¹ and 1.01–2.73 mmol L⁻¹, respectively; the C_{org} and C_{endo} values of springs along the East Kunlun fault zone are 0.67–4.18 mmol L⁻¹ and 1.17–13.90 mmol L⁻¹, respectively. For most springs of the East Kunlun fault zone, the average proportions of organic carbon, deeply-sourced carbon, and carbonate end-members are 18.6% (3.3–26.7%), 45.7% (35.9–67.4%) and 35.7% (29.3–42.8%), respectively (Table 2). In contrast, the spring waters in the Maduo surface rupture zone yield average end-member proportions of 28.1% (18.7–32.9%) for organic carbon, 30.7% (21.2–39.1%) for deeply-sourced carbon, and 41.2% (32.7–52.6%) for carbonate, respectively (Table 2). Irrespective of sample locations, the DIC in the studied spring waters are generally derived from dissolution of carbonates (average = 38.1%), followed by deeply-sourced carbon (average = 35.2%) and organic carbon (average = 26.7%). Notably, spring waters from the Maduo surface rupture zone have higher inputs from organic carbon (28.1%) than those from the East Kunlun fault

zone (18.6%), with the latter showing higher contributions from deeply-sourced carbon (45.7% vs. 30.7%).

5.3 Mechanism of earthquake-induced carbon mobilization

Previous studies have reported that anomalies in chemical compositions and isotope ratios of carbon-bearing fluids before and after seismic events could reflect earthquake-induced fluid release as well as changes in fluid migration pathways (e.g., Weise et al., 2001; Bräuer et al., 2007; Chiodini et al., 2011; Bräuer et al., 2014). Generally, the geochemical anomalies can be explained by fluid discharge from isolated pores and fractures, mixing of components from different aquifers, and increased inputs of surface flow or deeply-sourced fluids (Rosen et al., 2018; Barbieri et al., 2020).

In this study, springs in the Maduo surface rupture zone show more organic carbon contribution compared to most springs in the East Kunlun fault zone. These springs reflect the post-earthquake upwelling of mostly shallow groundwater and recharged surrounding water (Lu et al., 2021). Due to the

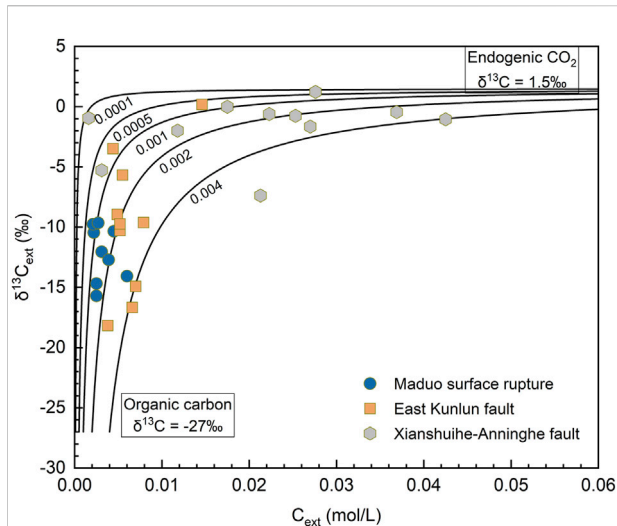


FIGURE 3

Plot of $\delta^{13}\text{C}_{\text{ext}}$ versus C_{ext} for spring samples in the study area. Data of the Xianshuihe-Anninghe fault zone are from Xu et al. (2022). The modeling parameters of end-members are as follows: (1) Organic carbon: $\delta^{13}\text{C}_{\text{org}} = -27\text{‰}$, $C_{\text{ext}} = 0.0001\text{--}0.004 \text{ mol L}^{-1}$; (2) Endogenic (deeply-sourced) carbon: $\delta^{13}\text{C}_{\text{endo}} = 1.5\text{‰}$, $C_{\text{ext}} \gg 0.06 \text{ mol L}^{-1}$. The $\delta^{13}\text{C}$ value of deeply-sourced carbon end-member represents a mixture of carbon from mantle degassing and decomposition of marine limestones. The $\delta^{13}\text{C}$ value of metamorphic CO_2 depends on that of source rocks, and we cannot discriminate carbon from mantle degassing and metamorphic decarbonation due to the lack of further geochemical data (e.g., $^3\text{He}/^4\text{He}$) in this study. The numbers (i.e., 0.0001, 0.0005, 0.001, 0.002, and 0.004) near corresponding mixing curves represent carbon contents (shown in C_{ext}) of organic carbon end-member.

mixing between surface water and groundwater in the rupture zone formed by the Maduo earthquake, we suggest that more modern soil CO_2 entered into the spring waters (Figure 4A), consistent with our carbon isotope results (Tables 1 and 2). Geophysical data show that the Jiangcuo fault, along which the Maduo earthquake occurred, mainly extends to the brittle upper

crustal depths (0–30 km; Yue et al., 2022), as indicated by the epicenter of about 17 km (Zhu et al., 2021). In this case, the inputs of deeply-sourced carbon would be less than those of shallow organic carbon and sedimentary carbonates. The enhanced release of organic carbon after earthquakes has also been observed in other seismically active regions (Wang et al., 2016; Bonini, 2022). For example, Rosen et al. (2018) reported a decrease in $\delta^{13}\text{C}_{\text{DIC}}$ values from -11.6‰ to -17.3‰ for the Nerea spring after the 2016 Amatrice-Norcia earthquake, which was probably due to soil CO_2 release. After the 2008 Wenchuan earthquake, Zheng et al. (2013) also observed emissions of biogenic gases from shallow reservoirs through faults or fractures.

As an important boundary fault of the Songpan-Ganzi block, the East Kunlun fault zone cut deep into the middle and lower crust (Sun et al., 2019), which is conducive to the upward migration of deep fluids. Therefore, most springs near the East Kunlun fault zone show high contributions from deeply-sourced carbon components as shown in Figure 4B. Similarly, after the 2016 Amatrice-Norcia earthquake, Rosen et al. (2018) observed an increase of $\delta^{13}\text{C}_{\text{DIC}}$ ($\sim 6\text{‰}$) in the Santa Susanna Spring. Such abrupt change was attributed to increased inputs from deeply-sourced carbon, or the addition of groundwater enriched in heavier carbon isotopes (such as the groundwater from reservoirs with long residence time or intense water-rock interaction). Notably, relatively higher organic carbon contributions are observed in three springs (MDW14, MDW15, and MDW16; Table 2) along the East Kunlun fault. Since their $\delta^{13}\text{C}_{\text{DIC}}$ values are similar to that of the Yellow River water (MDW8). It is possible that fluid sources of the three springs are influenced by shallow waters such as rivers or streams, which thus fails to reflect the deep fluid circulation related to deep-cutting nature of the East Kunlun fault zone.

The above findings suggest that seismic events such as the 2021 Maduo earthquake can affect carbon mobilization processes at variable depths, especially shallow organic carbon that tends to be released from the newly formed rupture zones (Figure 4). The

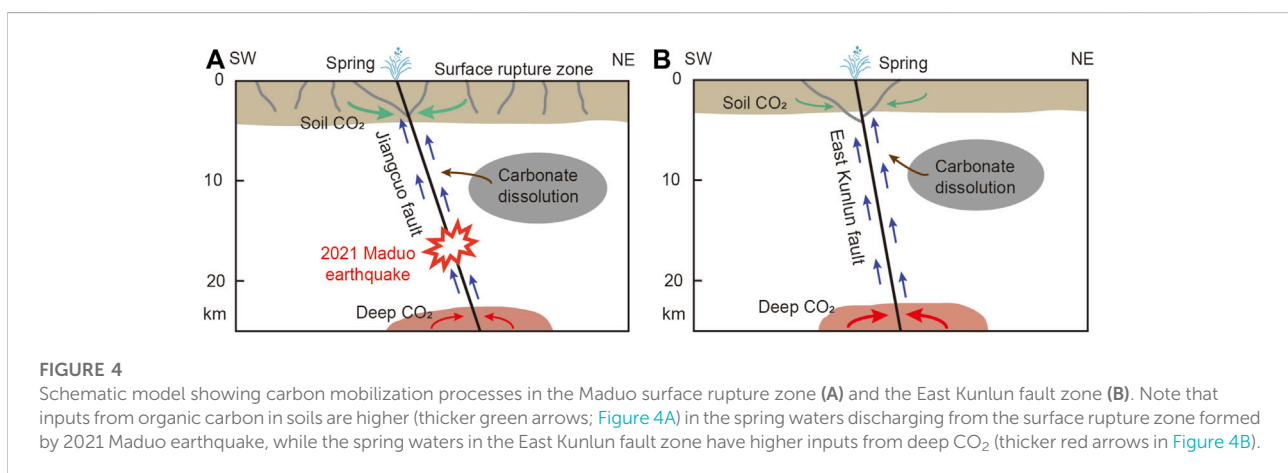


FIGURE 4

Schematic model showing carbon mobilization processes in the Maduo surface rupture zone (A) and the East Kunlun fault zone (B). Note that inputs from organic carbon in soils are higher (thicker green arrows; Figure 4A) in the spring waters discharging from the surface rupture zone formed by 2021 Maduo earthquake, while the spring waters in the East Kunlun fault zone have higher inputs from deep CO_2 (thicker red arrows in Figure 4B).

combination of changes in hydrogeochemical and isotopic signatures of groundwater before and after earthquake could further reveal the mechanism of carbon emissions induced by perturbations in carbon mobilization processes at deep and shallow levels (Rosen et al., 2018). Moreover, it is also of considerable significance to take into account the potential effects of earthquake-induced CO₂ emissions in modeling of tectonic evolution and carbon cycling over longer timescales (Wang et al., 2016).

6 Conclusion

Based on stable carbon isotope and radiocarbon isotope of the DIC in spring and surface waters, combined with regional geological and geophysical evidence, our study quantitatively constrained the carbon source components involved in the discharging subsurface fluids after the 2021 Maduo earthquake. Overall, the DIC in spring waters is mainly derived from dissolved carbonate minerals (38.1%), modern soil organic carbon (26.7%), and deeply-sourced carbon (35.2%). Spatially, spring waters discharging from the Maduo surface rupture zone have higher inputs from modern soil organic carbon (28.1%) than those observed in the East Kunlun fault zone (18.6%), suggesting enhanced mobilization of organic carbon as a result of earthquake-induced fault rupturing that is suggested to be confined within upper crustal depths. In contrast, the higher inputs of deeply-sourced carbon (45.7%) to spring waters from the East Kunlun fault zone suggest higher probability of decarbonation processes at larger depths in the case of deep cutting of the East Kunlun strike-slip fault system. We suggest that the earthquake-induced release of organic carbon, as indicated by our observations after the 2021 M_w 7.4 Maduo earthquake, could shed new insights into the potential relationships between tectonic evolution and global carbon cycle.

Data availability statement

The original contributions presented in the study are included in the article/Supplementary Material, further inquiries can be directed to the corresponding authors.

References

- Barbieri, M., Boschetti, T., Barberio, M. D., Billi, A., Franchini, S., Iacumin, P., et al. (2020). Tracing deep fluid source contribution to groundwater in an active seismic area (central Italy): A combined geothermometric and isotopic ($\delta^{13}\text{C}$) perspective. *J. Hydrol. X*, 582, 124495. doi:10.1016/j.jhydrol.2019.124495
- Becker, J. A., Bickle, M. J., Galy, A., and Holland, T. J. B. (2008). Himalayan metamorphic CO₂ fluxes: Quantitative constraints from hydrothermal springs. *Earth Planet. Sci. Lett.* 265, 616–629. doi:10.1016/j.epsl.2007.10.046
- Bonini, M. (2022). Can coseismic static stress changes sustain postseismic degassing? *Geology* 50, 371–376. doi:10.1130/G49465.1

Author contributions

SX and MZ conceived the study based on samples collected by XZ. YL analyzed the samples, performed data modeling, and wrote the manuscript with contributions from SX, MZ, WL, and JZ. WL helped with model visualization. SX and MZ revised the manuscript based on comments from other authors.

Funding

This work was supported by National Key Research and Development Project (Grant No. 2020YFA0607700) and National Natural Science Foundation of China (Grant Nos. 41930642 and 42072327). MZ is supported as an Overseas Researcher under a Postdoctoral Fellowship (Grant No. P20025) of the Japan Society for the Promotion of Science (JSPS).

Acknowledgments

Yue Zheng is appreciated for polishing English language of the draft manuscript. We thank editorial handling by Associate Editor Long Li and constructive comments and suggestions from Cyril Aubaud and Kan Li.

Conflict of interest

The authors declare that the research was conducted in the absence of any commercial or financial relationships that could be construed as a potential conflict of interest.

Publisher's note

All claims expressed in this article are solely those of the authors and do not necessarily represent those of their affiliated organizations, or those of the publisher, the editors and the reviewers. Any product that may be evaluated in this article, or claim that may be made by its manufacturer, is not guaranteed or endorsed by the publisher.

- Bräuer, K., Kämpf, H., Koch, U., Niedermann, S., and Strauch, G. (2007). Seismically induced changes of the fluid signature detected by a multi-isotope approach (He, CO₂, CH₄, N₂) at the Wettinquelle, Bad Brambach (central Europe). *J. Geophys. Res.* 112, B04307. doi:10.1029/2006JB004404

- Bräuer, K., Kämpf, H., and Strauch, G. (2014). Seismically triggered anomalies in the isotope signatures of mantle-derived gases detected at degassing sites along two neighboring faults in NW Bohemia, central Europe. *J. Geophys. Res. Solid Earth* 119, 5613–5632. doi:10.1002/2014JB011044

- Campeau, A., Wallin, M. B., Giesler, R., Löfgren, S., Mörth, C.-M., Schiff, S., et al. (2017). Multiple sources and sinks of dissolved inorganic carbon across Swedish

- streams, refocusing the lens of stable C isotopes. *Sci. Rep.* 7, 9158. doi:10.1038/s41598-017-09049-9
- Chiodini, G., Caliro, S., Cardellini, C., Frondini, F., Inguaggiato, S., and Matteucci, F. (2011). Geochemical evidence for and characterization of CO₂ rich gas sources in the epicentral area of the Abruzzo 2009 earthquakes. *Earth Planet. Sci. Lett.* 304, 389–398. doi:10.1016/j.epsl.2011.02.016
- Chiodini, G., Cardellini, C., Amato, A., Boschi, E., Caliro, S., Frondini, F., et al. (2004). Carbon dioxide Earth degassing and seismogenesis in central and southern Italy. *Geophys. Res. Lett.* 31, L07615. doi:10.1029/2004GL019480
- Chiodini, G., Frondini, F., Cardellini, C., Parello, F., and Peruzzi, L. (2000). Rate of diffuse carbon dioxide Earth degassing estimated from carbon balance of regional aquifers: The case of central apennine, Italy. *J. Geophys. Res.* 105, 8423–8434. doi:10.1029/1999JB900355
- Claesson, L., Skelton, A., Graham, C., Dietl, C., Mörth, M., Torssander, P., et al. (2004). Hydrogeochemical changes before and after a major earthquake. *Geol.* 32, 641–644. doi:10.1130/G20542.1
- Crossey, L. J., Karlstrom, K. E., Springer, A. E., Newell, D., Hilton, D. R., and Fischer, T. (2009). Degassing of mantle-derived CO₂ and He from springs in the southern Colorado plateau region—neotectonic connections and implications for groundwater systems. *Geol. Soc. Am. Bull.* 121, 1034–1053. doi:10.1130/b26394.1
- Faulkner, D. R., Jackson, C. A. L., Lunn, R. J., Schlische, R. W., Shipton, Z. K., Wibberley, C. A. J., et al. (2010). A review of recent developments concerning the structure, mechanics and fluid flow properties of fault zones. *J. Struct. Geol.* 32, 1557–1575. doi:10.1016/j.jsg.2010.06.009
- Girault, F., Adhikari, L. B., France-Lanord, C., Agrinier, P., Koirala, B. P., Bhattarai, M., et al. (2018). Persistent CO₂ emissions and hydrothermal unrest following the 2015 earthquake in Nepal. *Nat. Commun.* 9, 2956. doi:10.1038/s41467-018-05138-z
- Han, G., Han, W. S., Kim, K.-Y., Park, J. G., Piao, J., and Yun, T. K. (2019). Roles of fault structures and regional formations on CO₂ migration and distribution in shallow saline aquifer in Green River, Utah. *J. Hydrol. X.* 570, 786–801. doi:10.1016/j.jhydrol.2019.01.027
- Hoefs, J. (2009). *Stable isotope geochemistry*. Berlin: Springer-Verlag.
- Hubbard, J., and Shaw, J. H. (2009). Uplift of the longmen Shan and Tibetan plateau, and the 2008 wenchuan (M = 7.9) earthquake. *Nature* 458, 194–197. doi:10.1038/nature07837
- Ingebritsen, S. E., and Manga, M. (2014). Hydrogeochemical precursors. *Nat. Geosci.* 7, 697–698. doi:10.1038/ngeo2261
- Kulongoski, J. T., Hilton, D. R., Barry, P. H., Esser, B. K., Hillemonds, D., and Belitz, K. (2013). Volatile fluxes through the big bend section of the san andreas fault, California: Helium and carbon-dioxide systematics. *Chem. Geol.* 339, 92–102. doi:10.1016/j.chemgeo.2012.09.007
- Liu, M., and Stein, S. (2016). Mid-continental earthquakes: Spatiotemporal occurrences, causes, and hazards. *Earth. Sci. Rev.* 162, 364–386. doi:10.1016/j.earscirev.2016.09.016
- Liu, W., Guan, L., Liu, Y., Xie, X., Zhang, M., Chen, B., et al. (2022). Fluid geochemistry and geothermal anomaly along the Yushu-Ganzi-Xianshuihe fault system, eastern Tibetan Plateau: Implications for regional seismic activity. *J. Hydrol. X.* 607, 127554. doi:10.1016/j.jhydrol.2022.127554
- Lu, C., Zhou, X., Li, Y., Liu, L., Yan, Y., and Xu, Y. (2021). Hydrogeochemical characteristics of groundwater in the surface rupture zone of Madoi M_{7.4} earthquake and hot springs in the East Kunlun Fault. *Seismol. Geol.* 43, 1101–1126. In Chinese with English abstract. doi:10.3969/j.issn.0253-4967.2021.05.005
- Mayorga, E., Aufdenkampe, A. K., Masiello, C. A., Krusche, A. V., Hedges, J. I., Quay, P. D., et al. (2005). Young organic matter as a source of carbon dioxide outgassing from Amazonian rivers. *Nature* 436, 538–541. doi:10.1038/nature03880
- Miller, S. A., Collettini, C., Chiaraluca, L., Cocco, M., Barchi, M., and Kaus, B. J. P. (2004). Aftershocks driven by a high-pressure CO₂ source at depth. *Nature* 427, 724–727. doi:10.1038/nature02251
- Newell, D. L., Jessup, M. J., Cottle, J. M., Hilton, D. R., Sharp, Z. D., and Fischer, T. P. (2008). Aqueous and isotope geochemistry of mineral springs along the southern margin of the Tibetan plateau: Implications for fluid sources and regional degassing of CO₂. *Geochem. Geophys. Geosyst.* 9, Q08014. doi:10.1029/2008gc002021
- Pan, J., Li, H., Chevalier, M.-L., Tapponnier, P., Bai, M., Li, C., et al. (2022). Co-seismic rupture of the 2021, M_w7.4 Madoi earthquake (northern Tibet): Short-cutting of the Kunlun fault big bend. *Earth Planet. Sci. Lett.* 594, 117703. doi:10.1016/j.epsl.2022.117703
- Pineau, F., Shilobreeva, S., Hekinian, R., Bideau, D., and Javoy, M. (2004). Deep-sea explosive activity on the mid-atlantic ridge near 34°50'N: A stable isotope (C, H, O) study. *Chem. Geol.* 211, 159–175. doi:10.1016/j.chemgeo.2004.06.029
- Ren, J., Xu, X., Yeats, R. S., and Zhang, S. (2013). Millennial slip rates of the Tazang fault, the eastern termination of Kunlun fault: Implications for strain partitioning in eastern Tibet. *Tectonophysics* 608, 1180–1200. doi:10.1016/j.tecto.2013.06.026
- Rosen, M. R., Binda, G., Archer, C., Pozzi, A., Michetti, A. M., and Noble, P. J. (2018). Mechanisms of earthquake-induced chemical and fluid transport to carbonate groundwater springs after earthquakes. *Water Resour. Res.* 54, 5225–5244. doi:10.1029/2017WR022097
- Skelton, A., Andrén, M., Kristmannsdóttir, H., Stockmann, G., Mörth, C.-M., Sveinbjörnsdóttir, Á., et al. (2014). Changes in groundwater chemistry before two consecutive earthquakes in Iceland. *Nat. Geosci.* 7, 752–756. doi:10.1038/ngeo2250
- Sun, X., Zhan, Y., Zhao, L., Chen, X., Sun, J., Li, C., et al. (2019). Electrical structure of the Kunlun–Qinling fault system, northeastern Tibetan Plateau, inferred from 3-D inversion of magnetotelluric data. *J. Asian Earth Sci.* 181, 103910. doi:10.1016/j.jseas.2019.103910
- Tamburello, G., Pondrelli, S., Chiodini, G., and Rouwet, D. (2018). Global-scale control of extensional tectonics on CO₂ Earth degassing. *Nat. Commun.* 9, 4608. doi:10.1038/s41467-018-07087-z
- Tapponnier, P., Zhiqin, X., Roger, F., Meyer, B., Arnaud, N., Wittlinger, G., et al. (2001). Oblique stepwise rise and growth of the Tibet Plateau. *Science* 294, 1671–1677. doi:10.1126/science.105978
- Telmer, K., and Veizer, J. (1999). Carbon fluxes, pCO₂ and substrate weathering in a large northern river basin, Canada: Carbon isotope perspectives. *Chem. Geol.* 159, 61–86. doi:10.1016/S0009-2541(99)00034-0
- Tian, J., Pang, Z., Liao, D., and Zhou, X. (2021). Fluid geochemistry and its implications on the role of deep faults in the Genesis of high temperature systems in the eastern edge of the Qinghai Tibet Plateau. *Appl. Geochem.* 131, 105036. doi:10.1016/j.apgeochem.2021.105036
- Tsunogai, U., and Wakita, H. (1995). Precursory chemical changes in ground water: Kobe earthquake, Japan. *Science* 269, 61–63. doi:10.1126/science.269.5220.61
- Ünal-İmer, E., Uysal, I. T., Zhao, J.-X., Işık, V., Shulmeister, J., İmer, A., et al. (2016). CO₂ outburst events in relation to seismicity: Constraints from microscale geochronology, geochemistry of late Quaternary vein carbonates, SW Turkey. *Geochim. Cosmochim. Acta* 187, 21–40. doi:10.1016/j.gca.2016.05.006
- Wang, J., Jin, Z., Hilton, R. G., Zhang, F., Li, G., Densmore, A. L., et al. (2016). Earthquake-triggered increase in biospheric carbon export from a mountain belt. *Geology* 44, 471–474. doi:10.1130/G37533.1
- Wang, S.-L., Lin, Y.-S., Burr, G. S., Wang, P.-L., and Lin, L.-H. (2022). Radiocarbon and stable carbon isotope constraints on the propagation of vent CO₂ to fluid in the acidic Kueishantao shallow water hydrothermal system. *Geochem. Geophys. Geosyst.* 23, e2022GC010508. doi:10.1029/2022GC010508
- Weise, S. M., Bräuer, K., Kämpf, H., Strauch, G., and Koch, U. (2001). Transport of mantle volatiles through the crust traced by seismically released fluids: A natural experiment in the earthquake swarm area vogtland/NW bohemia, central europe. *Tectonophysics* 336, 137–150. doi:10.1016/S0040-1951(01)00098-1
- Williams, A. J., Crossey, L. J., Karlstrom, K. E., Newell, D., Person, M., and Woolsey, E. (2013). Hydrogeochemistry of the Middle Rio Grande aquifer system — fluid mixing and salinization of the Rio Grande due to fault inputs. *Chem. Geol.* 351, 281–298. doi:10.1016/j.chemgeo.2013.05.029
- Wu, C., Yin, A., Zuza, A. V., Zhang, J., Liu, W., and Ding, L. (2016). Pre-Cenozoic geologic history of the central and northern Tibetan Plateau and the role of Wilson cycles in constructing the Tethyan orogenic system. *Lithosphere* 8, 254–292. doi:10.1130/L494.1
- Xu, S., Guan, L., Zhang, M., Zhong, J., Liu, W., Xie, X. g., et al. (2022). Degassing of deep-sourced CO₂ from Xianshuihe-Anninghe fault zones in the eastern Tibetan Plateau. *Sci. China Earth Sci.* 65, 139–155. doi:10.1007/s11430-021-9810-x
- Yue, H., Shen, Z.-K., Zhao, Z., Wang, T., Cao, B., Li, Z., et al. (2022). Rupture process of the 2021 M_{7.4} Madoi earthquake and implication for deformation mode of the Songpan-Ganzi terrane in Tibetan Plateau. *Proc. Natl. Acad. Sci. U. S. A.* 119, e2116445119. doi:10.1073/pnas.2116445119
- Zhang, M., Guo, Z., Xu, S., Barry, P. H., Sano, Y., Zhang, L., et al. (2021). Linking deeply-sourced volatile emissions to plateau growth dynamics in southeastern Tibetan Plateau. *Nat. Commun.* 12, 4157. doi:10.1038/s41467-021-24415-y
- Zheng, G., Xu, S., Liang, S., Shi, P., and Zhao, J. (2013). Gas emission from the qingzhu river after the 2008 wenchuan earthquake, southwest China. *Chem. Geol.* 339, 187–193. doi:10.1016/j.chemgeo.2012.10.032
- Zhou, X., Wang, W., Chen, Z., Yi, L., Liu, L., Xie, C., et al. (2015). Hot spring gas geochemistry in Western sichuan province, China after the wenchuan ms 8.0 earthquake. *Terr. Atmos. Ocean. Sci.* 26, 361–373. TT. doi:10.3319/tao.2015.01.05.01(tt)
- Zhu, Y., Diao, F., Fu, Y., Liu, C., and Xiong, X. (2021). Slip rate of the seismogenic fault of the 2021 Madoi earthquake in Western China inferred from GPS observations. *Sci. China Earth Sci.* 64, 1363–1370. doi:10.1007/s11430-021-9808-0
- Zucchi, M. (2020). Faults controlling geothermal fluid flow in low permeability rock volumes: An example from the exhumed geothermal system of eastern Elba Island (northern Tyrrhenian Sea, Italy). *Geothermics* 85, 101765. doi:10.1016/j.geothermics.2019.101765